IEEE Access
Multidisciplinary | Rapid Review | Open Access Journal

Received March 22, 2019, accepted May 3, 2019, date of publication June 13, 2019, date of current version July 11, 2019.

Digital Object Identifier 10.1109/ACCESS.2019.2922835

Analyzing Space Debris Flux and Predicting Satellites Collision Probability in LEO Orbits Based on Petri Nets

MOHAMED TORKY[1,4], ABOUL ELLA HASSANEIN[2,4], AHMED H. EL FIKY[3,4], AND YAZEED ALSBOU[5]

[1]Department of Computer Science, Higher Institute of Computer Science and Information Systems, Giza, Egypt
[2]Faculty of Computers and Information, Cairo University, Giza, Egypt
[3]Faculty of Engineering, Helwan University, Helwan, Egypt
[4]Scientific Research Group in Egypt (SRGE)
[5]Applied Science University, Al Eker, Bahrain

Corresponding author: Aboul Ella Hassanein (aboitcairo@gmail.com)

This work was supported by Egypt Knowledge and Technology Alliance (E-KTA) for Space Science, which is supported by The Academy of Scientific Research & Technology (ASRT), and coordinated by National Authority for Remote Sensing and Space Sciences (NARSS), (TEDDSAT Project grant).

ABSTRACT Space debris is rapidly becoming a real challenge and a serious threat for satellites and spacecraft motion. Most of these debris moves so fast, especially in the low earth orbits (LEOs) and so quickly that these debris can collide and penetrate the structure of the spacecraft and crash with the satellites. The National Aeronautics and Space Administration (NASA) expects that there will be an increase in the number of space particles in LEO orbits of 75% over the next 200 years if the space debris reduction measures are not followed. In this paper, we introduce the Petri net model for simulating the space debris flux estimation in the satellite orbits with respect to different debris sizes. Moreover, another Petri net model is introduced for investigating the impacts of debris flux on predicting the satellite collision probabilities. The analysis results show that there are negative correlations of the debris flux growth with the debris size d and the solar radio flux $F_{10.7}$. Moreover, the results clarify that the satellites in the LEO orbit at altitudes (h) of 600 km $< h <$ 1000 km and the inclination angles (i) of 900 $< i <$ 1000 cm are expected to experience more frequent collisions by 2030.

INDEX TERMS Space debris, flux distribution, collision probability, petri nets.

I. INTRODUCTION

Due to the growth rate of space operations such as launching satellites and spacecraft, very large amounts of resulting space debris will eventually pose serious challenges to near- Earth space activities without additional analysis and in depth research. Recent studies have demonstrated that there are approximately 5.5 million kilograms of human waste from Earth's orbits. Approximately one million particles are larger than one millimeter, more than 300,000 particles are larger than 1 centimeter, and more than 13,000 particles are larger than a tennis ball. NASA expects that there will be an increase in the number of space particles in low Earth Orbits (LEO) of 75 % over the next 200 years if space debris reduction measures are not followed [1], [2]. Orbital space debris can be produced from mission related debris, rocket bodies, spacecraft and fragmentation debris. As reported in the National Aeronautics and Space Administration (NASA), Orbital Debris Quarterly News in February 2018 [3], mission related debris, rocket bodies, spacecraft, and fragmentation debris represent 10%, 10%, 24%, and 56% of the total debris respectively. As a result of historical space operations and fragmentation, it is likely that the density of space particles has reached a critical level, where the rapid growth of space debris will continue with increase in human work in space. Debris growth comes from a widely-expected increase in the number of collisions between a large number of space masses. Most of these debris move at 8 km /s (approximately 28,800 km / h) in near-Earth orbits, and therefore, these debris can penetrate the structures of spacecraft and pose a threat to the lives of astronauts. Moreover, collisions with space debris can crash satellites

The associate editor coordinating the review of this manuscript and approving it for publication was Zheng H. Zhu.

or deviate them from their valid orbits. It is estimated that a pea-sized body travels so fast (100 km/h (60 m/h)) that it has a collision force equal to a body weight of 181 kilograms (400 pounds). Additionally, a volley of tennis-sized debris is so fast that it has a detonating capacity equal to 25 sticks of dynamite. Although more efforts have been paid and are still being paid by international space agencies such as NASA to generate more accurate estimates of how much space debris exists in space, evaluating and preventing space debris collisions need to be conducted more. Calculating collision probability with space debris is a very important stage for planning debris avoidance manoeuvres. Moreover, it is one of the most frequently stated problems with space debris collision avoidance mechanisms. The literature on estimating collision probability between spacecraft and orbital space debris has highlighted several methodologies and approaches based on different assumptions [5], [6]. Some methods evaluate the collision probability based on calculating the integral of the probability distribution function with assumed linear motion [9]–[11]. Other methods have evaluated the collision probability based on nonlinear relative motions [6], [12]. What we know about estimating the collision probability between space objects is largely based upon mathematical models that investigate how to use the geometrical vectors of orbital space objects to study their effects on collision probability calculations. Denenberg and Gurfil [13] developed a collision avoidance manoeuvre evaluation technique for a satellite cluster flight. The authors depended on information about the relative position (r_d) of space objects, and covariance matrices C_2D and C_3D for calculating the maximum collision probability function used to calculate the optimal debris avoidance manoeuvre for a specific satellite in the cluster. The collision probability P_c between two space particles in conjunction is also one of the most important criteria for conjunction risk assessment. Chen *et al.* [14] calculated the collision probability based on position and velocity vectors and the associated error covariance matrix. The authors derived the explicit expressions of the collision probability in terms of vectors of the relative position or the conjunction geometries in the cases of circular orbit and general orbit based on the closest approach analysis and estimation.

Calculating the collision probability based on nonlinear motion is another approach. Patera [6], [15] introduced a novel methodology that can be applied to low-velocity space vehicle encounters that involve nonlinear relative motion. The method calculated the collision probability of nonlinear relative motion based on the change in relative velocity and the error covariance matrices over time. The method has been validated using the nonlinear encounter between two geosynchronous satellites. The obtained results were compared with those generated via Monte Carlo simulation, and the nonlinear model results differed by only 2% from the results obtained using 6000 Monte Carlo runs. Moreover, Alfano [12] proposed another two proposed methodologies for calculating space collision probability based on nonlinear relative motion. The first method calculated the collision probability by extending linear methods to represent the collision tube as a series of adjoining tubes in Cartesian space. The second method represents the collision tube as voxels in Mahalanobis space. The method-analysis showed that apparent motion in Cartesian space can be misleading when working in Mahalanobis space.

Other studies have addressed the space collision probability problem by the Adaptive Splitting Technique (AST) [16]. Pastel [17] discussed the possibility of estimating satellite versus debris collision probabilities via the AST, which was also compared with the Crude Monte Carlo method, and the results clarified the superiority of the AST. The collision probability can also be calculated by analyzing the space debris flux distribution with the space station. Liu and Zhu [18] evaluated the collision probability between the space station and space debris based on the micrometeoroid environmental model in the NASA SSP 30425B standard [19]. The simulation results demonstrated a high probability of collisions for space debris sizes concentrated below 0.1 mm but probability of collisions for other sizes of debris was very low and close to zero. However these results may not be sound because the authors built the collision probability calculations based on micro-meteoroid environmental models rather than debris models. Such that, Estimating collision probability based on Micro-meteoroids environmental models requires to convert the flux of the interstellar micro-meteoroid into earth orbital micro-meteoroid flux. This requires the consideration of Earth's shielding effect and the gravitational convergence effect that can play a role in reducing the flux of micro-meteoroids. Moreover, Micrometeoroids are smaller than space debris, such that space debris may be found in different sizes. Hence, the dependence on Micro-meteoroids environmental models may not be accurate enough for estimating different patterns of space debris that may obstacle the spacecraft and satellites in different orbits at different altitudes and at inclination angles. Analyzing space debris based on the reported results from the NASA orbital debris evolutionary model, LEGEND is another method for estimating collision actions in the future orbital debris environment [20], [21]. The simulation results showed that most LEO collisions occur in regions of high spatial density, around 800 and 1000 km altitudes. Moreover, the authors claimed that it is a critical thing to have a high accurate model to analyze future collision activities to ensure reliable environment predictions. However, the new capabilities of LEGEND model may support to investigate the process in a better way and provides more understanding of the collisions nature. Moreover, Liou [22] introduced an additional analysis approach from 200 Monte Carlo simulations for predicting in more convincing the future debris environment using the NASA long-term orbital debris evolutionary model LEGEND.

Although many tries are introduced for cleaning the satellites-orbits from debris, removing space debris is still represents a big challenge against space agencies.

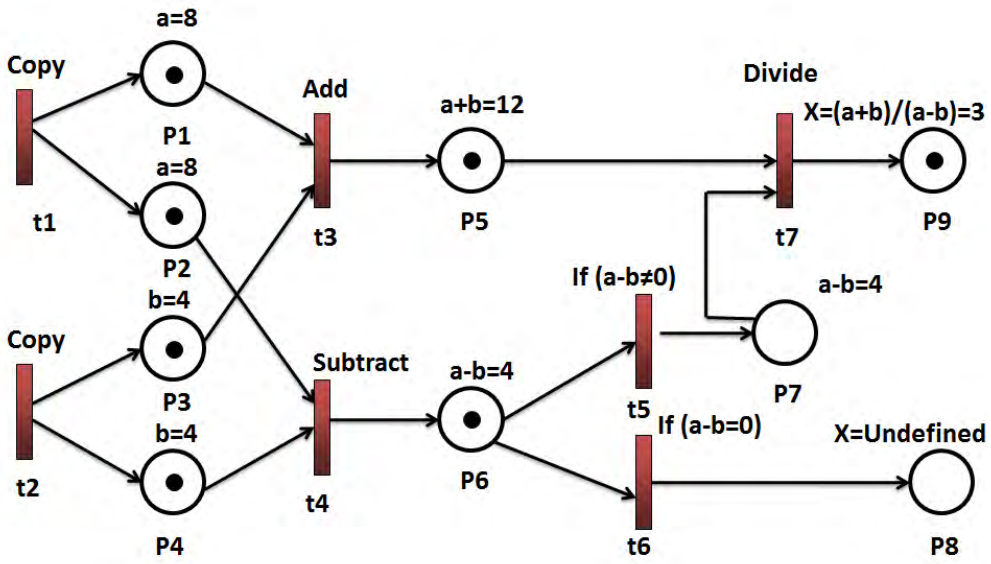

FIGURE 1. Petri net example.

Some research studies tried to propose set of countermeasures for suppressing space debris growth based on electro-dynamic tether system [23], [24]. Moreover, The Institute of Aerospace Technology (IAT) and Japan Aerospace Exploration Agency (JAXA), are studying a micro-satellite system for active space debris removal, and are examining the applicability of electro-dynamic tether (EDT) technology as its high efficiency orbital transfer system [25]. Space debris removal using Ion Beam technology is another effective methodology for cleaning satellites orbits from space debris [26], [27]. Moreover, the development of a novel fiber based laser architectures is considerable approaches for space debris removal [28], [29]. Such a new architecture has been developed by the International Coherent Amplification Network (ICAN) which has been analyzed for the purpose of tracking and de-orbiting hyper-velocity space debris [30].

In this paper, the flux distribution of space debris moving towards a satellite's orbit is investigated and mathematically estimated, analyzed, and simulated by a Petri net model. The flux distribution of space debris is based on the Space Station Program (SSP) 30425B standard [19]. Moreover, another Petri net model is proposed for predicting the expected number of collisions and the corresponding probability values of collisions between a specific satellite and space debris. The simulated method by this model is based on the flux distribution of space debris within a specific year and some orbital attributes of the threatened satellite that affect the collision prediction calculations. The proposed approach is applied to a set of well-known LEO satellites that have different orbital attributes for evaluating the effectiveness of the proposed approach in predicting collision probability values within the next 12 years. The rest of this paper can be organized as follows: section 2 presents a short background on Petri nets. section 3 discusses the flux distribution analysis of space debris by a Petri net model, section 4 introduces another Petri net model for predicting collision probability between satellites and space debris, section 5 presents the analysis results, section 6 discusses the obtained results, and section 7 presents a general conclusion of this study.

II. PETRI NETS: AN OVERVIEW

Petri nets are mathematical and graphical modeling tools that can be used for modeling and simulating the behaviors of many systems. As a graphical tool, Petri nets are weighted and bipartite graphs consisting of two kinds of nodes, *places* in the form circles and *transitions* in boxes or bars [31]. The arcs must be either from a place to a transition or from a transition to a place. Places work as repositories of data, and the transitions work as algorithms, or functions of that data. A specific Petri net model changes its state (i.e, new markings) according to tokens (i.e, black dots) residing in all places in each state. The behavior of any system that modeled by a Petri net model, can be described by the number of states. States simulate the changes and dynamic behavior of a system. A state or marking in the Petri net model is changed according to the following firing rules: (1) a transition, t, is said to be enabled if each input place p of t is marked with at least $w(p, t)$ tokens, where $w(p, t)$ represents the weight of the arc from p to t. (2) An enabled transition, t, may or may not fire depending on whether the event actually takes place. (3) The firing of an enabled transition t removes $w(t, p)$ tokens from each input place p of t and adds $w(t, p)$ tokens to each output place p of t, where $w(t, p)$ represents the weight of the arc from t to p. The transition t without an input place is called a source transition which is unconditionally enabled. Figure 1 depicts an example of the Petri Net model for calculating the value of the expression: $X = (a + b)/(a - b)$. Firing the source transitions $t1$, and $t2$ produce a, and b values respectively. Firing $t3$ executes the *addition* operation and produces the resulting token in place $P5$. Firing $t4$ executes

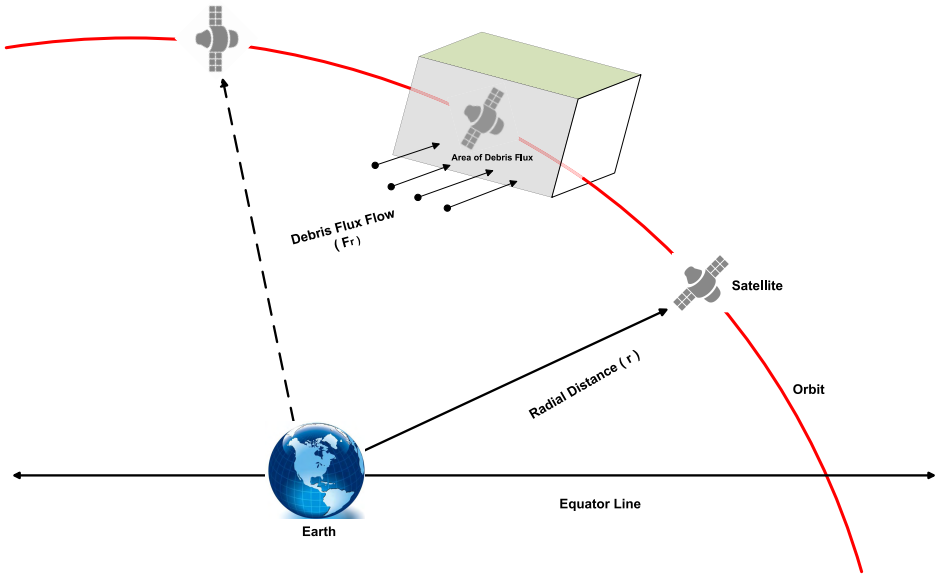

FIGURE 2. Debris flux against satellite orbit.

the *subtraction* operation and produces the resulting token in place $P6$. Firing $t5$ is conditioned with the boolean expression $a - b \neq 0$ with respect to the token value in $P6$, and Firing $t6$ is conditioned with the boolean expression $a - b = 0$ with respect to the token value in $P6$. If $t5$ fires, it produces the resulting token value in $P7$, In this state, $t7$ becomes enabled; then firing it calculates the value of the expression: $X = (a+b)/(a-b)$ with respect to the token values in $P5$, and $P7$ produces the resulting token value in $P9$; otherwise, firing $t6$ produces an undefined token value for X in $P8$. In this study, two Petri net models are proposed. The first model can be used to simulate the debris flux distribution in LEO orbits, and the second model can be used to estimate the collision probability between satellites and debris in LEO orbits. The main advantage of using Petri nets here is its efficiency in simulating and modeling the complex calculations of debris flux evaluation and predicting the probability of collision in a visualized and graphical form. Moreover, the prediction calculations of space debris flux growth and collision with spacecraft is a concurrent and data driven process, hence, Petri Nets is the best modeling tool for simulating such type of systems and capture the interactions and processing of concurrent and sequential data.

III. DEBRIS FLUX ANALYSIS MODEL

One of the recent methods for estimating and analyzing the orbital space debris environment is calculating the flux distribution of the space debris function F_r. Calculating the F_r function is considered a base requirement for determining the collision probability between satellites and orbital space debris. To analyze the debris flux distribution in space, we should imagine that at any point in the orbit in which the satellite passes, debris can collide with the satellite through six surfaces, as depicted in Figure 2. In the most recent studies, the flux distribution function F_r has been measured based on a micrometeoroid environmental model [18], which is also based on the NASA SSP30425 standard [19]. However, this method depends on micrometeoroid features and variables rather than debris features and variables. Hence, the evaluation results may be inaccurate. In this study, we use the debris flux distribution model instead of the micrometeoroid flux distribution. The model used is also based on the NASA SSP30425 standard [19]. The major advantages of using the debris flux distribution model are that (1) the current debris environment investigation was analyzed based on the best experimental data available. The panels of these data have been returned from the Solar Max satellite, the optical measurements by the Massachusetts Institute of Technology (MIT) using their experimental test site (ETS) telescopes, and U.S. Space Command catalogued and un catalogued data sets. (2) This model can represent a projection of the change in the anticipated debris environment over the upcoming years. The cumulative flux Fr distribution of the orbital debris sizes with diameter d is given by equation 1 [19]:

$$F_r(d, h, i, t, S) = \lambda \times \mu \tag{1}$$

where, F_r represents the debris flux ($pieces/m^2/year$), d represents the debris diameter in cm, h represents the altitude in km ($h < 2000\ km$), i represents the inclination angle in degrees, t represents the date (year), and S represents the solar radio flux $F_{10.7}$ for $t - 1$ year, λ, and μ are defined as in

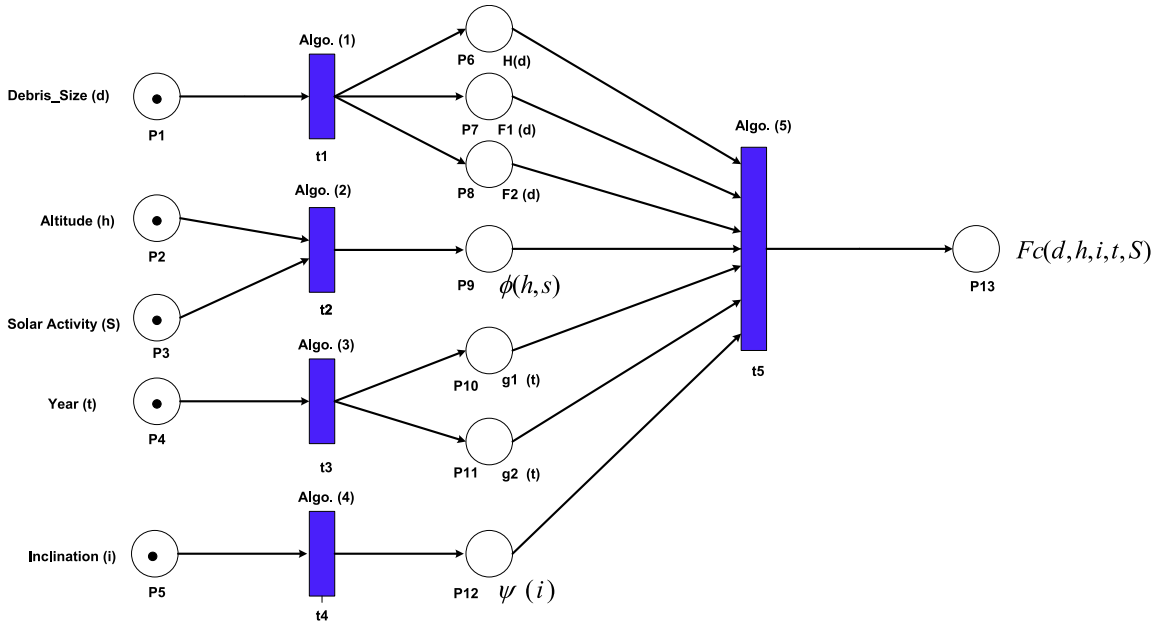

FIGURE 3. Petri net model for evaluating debris flux in LEO orbits.

equations 2, and 3 respectively [32].

$$\lambda = H(d).\phi(h,S).\Psi(i) \tag{2}$$

$$\mu = [F_1(d).g_1(t) + F_2(d).g_2(t)] \tag{3}$$

where $\Psi(i)$ represents the inclination dependent function, and $H(d)$, $\phi(h,S)$, $\psi_1(h,s)$, $F_1(d)$, $F_2(d)$, $g_1(t)$, and $g_2(t)$ are defined in equations 4,5,6,7,8,9,and 10 respectively.

$$H(d) = [10^{exp(-(\log d - 0.78)^2/0.637^2)}]^{1/2} \tag{4}$$

$$\phi(h,S) = \psi_1(h,s)/(\psi_1(h,s)+1) \tag{5}$$

$$\psi_1(h,s) = 10^{(\frac{h}{200} - \frac{S}{140} - 1.5)} \tag{6}$$

$$F_1(d) = 1.22 \times 10^{-5} d^{-2.5} \tag{7}$$

$$F_2(d) = 8.1 \times 10^{10} (d+700)^{-6} \tag{8}$$

$$g_1(t) = \begin{cases} (1+q)^{t-1988}, & \text{t} < 2011. \\ (1+q)^{23}(1+\tilde{q})^{t-2011}, & \text{t} \geq 2011. \end{cases} \tag{9}$$

where, q and $\tilde{q}$ represent the estimated growth rates of fragments; $q = 0.02$; and $\tilde{q} = 0.04$ respectively.

$$g_2(t) = 1 + [p.(t - 1988)] \tag{10}$$

where, p represents the assumed annual growth rate of intact objects in orbit, $p = 0.05$

The debris flux through six surfaces $F_C(d,h,i,t,S)$ around a threatened satellite can be calculated as shown in equation 11.

$$F_C(d,h,i,t,S) = 6 \times F_r(d,h,i,t,S). \tag{11}$$

Estimating the total debris flux TDF_{orbit} in a specific orbit within an identified year can be calculated based on the length of the orbit L_{orbit}. TDF_{orbit} can be estimated as shown in Equation 12

$$TDF_{orbit} = L_{orbit} \times F_C(d,h,i,t,S) \tag{12}$$

Estimating the length of orbit L_{orbit} is based on whether it is a circular orbit or elliptical orbit. The length of circular orbits can be estimated as shown in equation 13, while, the length of elliptical orbits can be estimated as shown in equation 14.

$$L_{orbit} = 2\pi r \tag{13}$$

where, r represents the radial distance from Earth to the position of the satellite on the circular orbit

$$L_{orbit} \approx \pi[3(a+b) - \sqrt{(3a+b)(a+3b)}] \tag{14}$$

where, a represents the semi major axis and b represents the semi minor axis of the elliptical orbit.

The debris flux evaluation method can be simulated using a Petri net model as depicted in Figure 3.

The model consist of 13 places and 5 transitions. Firing $t1$ calculates $H(d)$, $F_1(d)$, and $F_2(d)$ based on the input debris size d and produces its token values in the places P_6, P_7, and P_8 respectively as depicted in algorithm (1). Firing $t2$ calculates $\phi(h,S)$ based on the inputs: orbit altitude (h) and (S), (solar radio flux $F_{10.7}$) for year $t-1$, then produces a $\phi(h,S)$ token value in P_9 as depicted in algorithm (2). Firing $t3$ calculates $g_1(t)$ and $g_2(t)$ based on the input year date (t) and produces its token values in places P_{10}, P_{11} respectively, as depicted in algorithm (3). Firing $t4$ specifies the inclination dependent function $\Psi(i)$ based on the input inclination angle (i) of the orbit and produces its token values in P_{12} as depicted in algorithm (4). Firing $t5$ produces the debris flux F_C token value in P_{13} as depicted in algorithm (5).

Algorithm 1 Firing Transition $t1$

Input: $Debris - Size(d)$
Output:: $H(d)$, $F_1(d)$, and $F_2(d)$
procedure Firing $t1$
    $H(d) = [10^{exp(-(\log d - 0.78)^2/0.637^2)}]^{1/2}$
    $F_1(d) = 1.22 \times 10^{-5} d^{-2.5}$
    $F_2(d) = 8.1 \times 10^{10}(d + 700)^{-6}$
return $H(d)$, $F_1(d)$, and$F_2(d)$
end procedure

Algorithm 2 Firing Transition $t2$

Input: Altitude (h), solar radio flux $F_{10.7}$ for $t - 1$ year (S)
Output:: $\phi(h, S)$
procedure Firing $t2$
    $\psi_1(h, s) = 10^{(\frac{h}{200} - \frac{S}{140} - 1.5)}$
    $\phi(h, S) = \psi_1(h, s)/(\psi_1(h, s) + 1)$
return $\phi(h, S)$
end procedure

Algorithm 3 Firing Transition $t3$

Input: year (t), $q = 0.02$; $\tilde{q} = 0.04$;$p = 0.5$
Output: $g_1(t)$, and $g_2(t)$
procedure Firing $t3$
    if t < 2011 **then**
        $g_1(t) = (1 + q)^{t-1988}$
    else
        $g_1(t) = (1 + q)^{23}(1 + \tilde{q})^{t-2011}$
    end if
    $g_2(t) = 1 + [p.(t - 1988)]$
return $g_1(t)$, $g_2(t)$
end procedure

Algorithm 4 Firing Transition $t4$

Input: Inclination (i)
Output: $\Psi(i)$
procedure Firing $t4$
    $Switch(i)$
    $i \approx 28.5 \Rightarrow \Psi(i) = 0.91$
    $i \approx 30 \Rightarrow \Psi(i) = 0.92$
    $i \approx 40 \Rightarrow \Psi(i) = 0.96$
    $i \approx 50 \Rightarrow \Psi(i) = 1.02$
    $i \approx 60 \Rightarrow \Psi(i) = 1.09$
    $i \approx 70 \Rightarrow \Psi(i) = 1.26$
    $i \approx 80 \Rightarrow \Psi(i) = 1.71$
    $i \approx 90 \Rightarrow \Psi(i) = 1.37$
    $i \approx 100 \Rightarrow \Psi(i) = 1.78$
    $i \approx 120 \Rightarrow \Psi(i) = 1.18$
return $\Psi(i)$
end procedure

Algorithm 5 Firing Transition $t5$

Input: $H(d)$, $F_1(d)$, $F_2(d)$
Input: $\phi(h, S)$, $g_1(t)$, $g_2(t)$, $\Psi(i)$
Output: : $F_C(d, h, i, t, S)$
procedure Firing $t5$
    $\lambda = H(d).\phi(h, S).\Psi(i)$
    $\mu = [F_1(d).g_1(t) + F_2(d).g_2(t)]$
    $F_r(d, h, i, t, S) = \lambda \times \mu$
    $F_C(d) = 6 \times F_r(d, h, i, t, S)$.
return $F_C(d, h, i, t, S)$
end procedure

IV. COLLISION PROBABILITY MODEL

It is hypothesized that the number of space debris collisions with spacecraft increases linearly with the space debris flux F_C, exposure cubic area A around the satellite, and exposure time T. Therefore, for simply evaluating the expected number of collisions N, the specific satellite may made in cubic area A ($1m^3$) in a specific year T can be estimated as shown in equation 15.

In addition, for estimating the total number of expected collisions N_{Total} along the length of the satellite's orbit within a specific year, equation 12 should be reformulated as shown in equation 16.

$$N = F_C \times A \times T \tag{15}$$

$$N_{Total} = L_{orbit} \times F_C \times A \times T \tag{16}$$

Once, the total number of expected collisions N_{Total} is determined, the collision probability distribution P_n that occurs n times in the corresponding year follows a Poisson distribution according to N_{Total} as shown in equation 17 [18].

$$P_n = \frac{N_{Total}^n \times e^{-N_{Total}}}{n!} \tag{17}$$

The non-collision probability can be estimated as shown in equation 18, while, the collision probability Q can be formulated in equation 19.

$$P_0 = e^{-N_{Total}} \tag{18}$$

$$Q = 1 - e^{-N_{Total}} \tag{19}$$

we used the Poisson distribution since it is a discrete probability distribution that expresses the probability of a given number of events occurring in a fixed interval of time. Here, the events is the satellite collisions and the fixed interval time is the period from 2019-2030.

Calculating the collision probability can also be simulated by the proposed Petri net model depicted in Figure 4.

Firing $t6$ calculates the length of the satellite orbit L_{Orbit} based on apogee and perigee input values of its orbit as shown in algorithm 6. Firing $t7$ calculates the expected number of collisions N_{Total} that a given satellite can experience in a given time interval T based on the length of the satellite's orbit L_{Orbit}, and the average flux of debris sizes $AVG(Fc)$ as

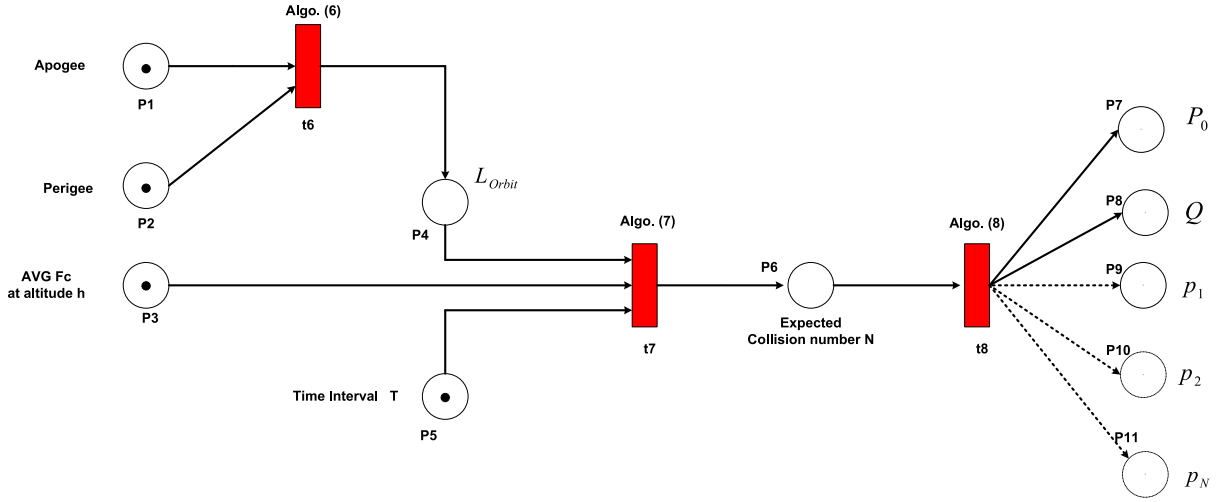

FIGURE 4. Petri net model for predicting the satellite/debris collision probability.

Algorithm 6 Firing Transition $t6$

Input: $Apogee(A)$, $Perigee(P)$
Input: $Veolicty(V)$, $PeriodT$
Output: : L_{Orbit}
procedure Firing $t6$
  $R_A = A + 6378$
  $R_P = P + 6378$
  $Eccentricity(e) = \frac{R_A - R_P}{R_A + R_P}$
  if e==0 **then**
  {
    $r = \frac{V \times T}{2\pi}$
    $L_{Orbit} = 2\pi r$
  }
  else
  {
    $a = \frac{R_A + R_P}{2}$
    $b = a.\sqrt{1 - e^2}$
    $L_{Orbit} = [3(a + b) - \sqrt{(3a + b)(a + 3b)}]$
  }
  end if
return L_{Orbit}
end procedure

Algorithm 7 Firing Transition $t7$

Input: L_{Orbit}, $AVG\ (Fc)$
Input: $TimeInterval\ (T)$, $CubicArea\ A$
Output: : $ExpectedCollisionNumber\ \ N_{Total}$
procedure Firing $t7$
  $N_{Total} = L_{Orbit} \times AVG(F_C) \times A \times T$
return N_{Total}
end procedure

detailed in algorithm 7. Firing $t8$ calculates the probability of collisions that the satellite can experience based on the input value of N_{Total} as depicted in algorithm 8.

Algorithm 8 Firing Transition $t8$

Input: N_{Total}, $n = 0$
Output:: P_n, Q
procedure Firing $t8$
  while n $\leq N_{Total}$ **do**
    $P_n = \frac{N_{Total}^n \times e^{-N_{Total}}}{n!}$
  end while
  $Q = 1 - P_0$
return P_n, Q
end procedure

V. RESULTS ANALYSIS

We have designed and implemented two applications for the two proposed Petri net models in C#. The first application is used to estimate the debris flux distribution F_C. The second application can be used to predict the expected number of collisions N_{Total} and estimate the corresponding probability of collision. In this section, we present an investigation of the two types of analysis. In subsection 5.1, we present the statistical analysis results of the debris flux growth based on the introduced debris flux analysis model. The analysis results were investigated based on different debris sizes at different inclination angles in LEO orbits at altitudes less than 1000 km within the period from 2019 to 2030. In subsection 5.2, the results of applying the collision probability model to a dataset with eight satellites (see Table 1) at different altitudes are presented and explained. The orbital attributes of each satellite in Table 1 have been gathered from Wikipedia.

A. DEBRIS FLUX GROWTH ANALYSIS RESULTS

The main advantage of the introduced Petri net model for debris flux growth is that it can be used to predict debris growth in LEO orbits, at any altitude of 200 $km \leq h \leq 2000\ km$ over different inclination angles ($28.5^o \leq i \leq 120^o$)

TABLE 1. Dataset description of eight satellite.

Satellite	Apogee(km)	Perigee (km)	inclination
EnviSat	774	772	98.40
ISS	406	403	51.64
GRACESat	508	483	89
TiangongSat 2	378.4	369	42.79
AQUASat	703	702	98
EO-1 Sat	700	690	98.7
ICE Sat	594	586	94
Suomi NPP	834.3	833.7	98.7

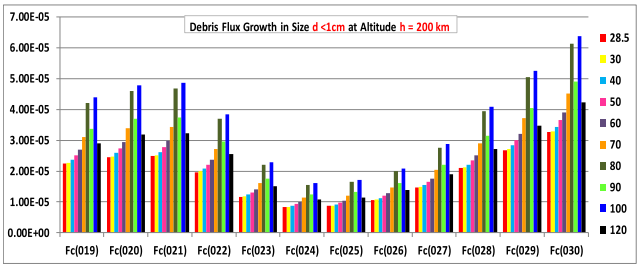

FIGURE 5. debris flux growth of size $d < 1cm$ at altitude $h = 200\ km$ at inclination angles from 28.5 to 120^0.

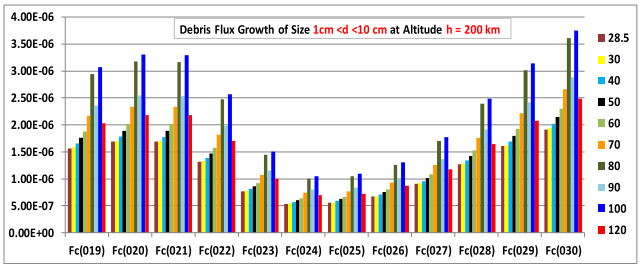

FIGURE 6. debris flux growth of size $1\ cm < d < 10cm$ at altitude $h = 200\ km$ at inclination angles from 28.5^0 to 120^0.

within any year. However, in this study, the analysis results only explains the debris flux growth within the period from 2019 to 2030 as we could not obtain the solar radio flux $F_{10.7}$ in years after 2030. Additionally, the analysis only focused on debris at altitudes of $200\ km \leq h \leq 1000\ km$ since it is assumed that debris is denser at these altitudes. We categorized space debris into six categories, according to the debris size d as follows:

1) $d < 1\ cm$,
2) $1\ cm < d < 10\ cm$
3) $10\ cm < d < 30\ cm$,
4) $30\ cm < d < 70\ cm$
5) $70\ cm < d < 120\ cm$
6) $d > 120\ cm$

From each category, we selected the following debris sizes samples: $d = 0.8\ cm$, $d = 5\ cm$, $d = 20\ cm$, $d = 50\ cm$, $d = 100\ cm$, and $d = 140\ cm$.

After applying and simulating the debris flux analysis Petri net model, figures 5, 6, 7, 8, 9 and 10 depict debris flux growth of the six categories of debris sizes from $d < 1\ cm$ to $d > 120\ cm$ respectively at the altitude $h = 200\ km$.

As shown in these figures, there is a direct impact of solar radio flux $F_{10.7}$ on the debris flux growth for the six debris

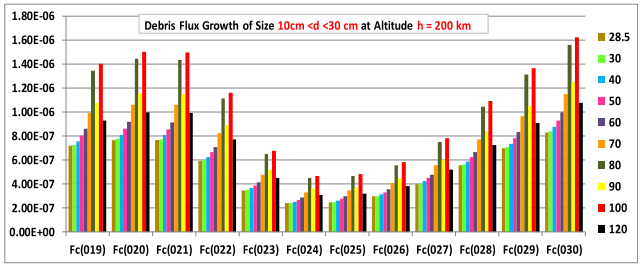

FIGURE 7. debris flux growth of size $10\ cm < d < 30cm$ at altitude $h = 200\ km$ at inclination angles from 28.5^0 to 120^0.

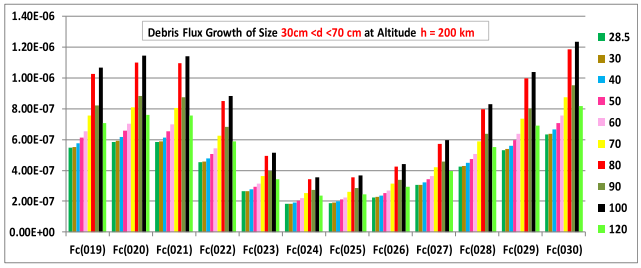

FIGURE 8. debris flux growth of size $30\ cm < d < 70cm$ at altitude $h = 200\ km$ at inclination angles from 28.5^0 to 120^0.

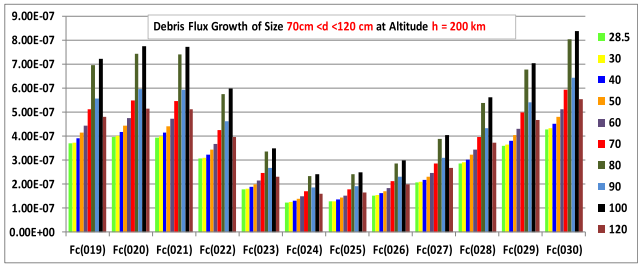

FIGURE 9. debris flux growth of size $70\ cm < d < 120cm$ at altitude $h = 200\ km$ at inclination angles from 28.5^0 to 120^0.

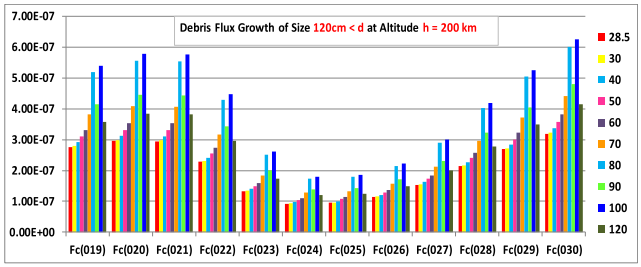

FIGURE 10. debris flux growth of size $120\ cm < d$ at altitude $h = 200\ km$ at inclination angles from 28.5^0 to 120^0.

size patterns in low altitudes within the next 11 years. There is a clear tendency of decreasing the debris flux at the altitude of $h = 200\ km$ within the years 2023-2026 because of the increasing values of the solar radio flux $F_{10.7}$ within these years. Moreover, these findings show an increasing growth of the debris flux F_C for the six debris size patterns at low altitudes by 2030. In addition, this results clarify that, all debris sizes classes are denser at the inclination angles 80^0 and 100^0 than other inclination angles.

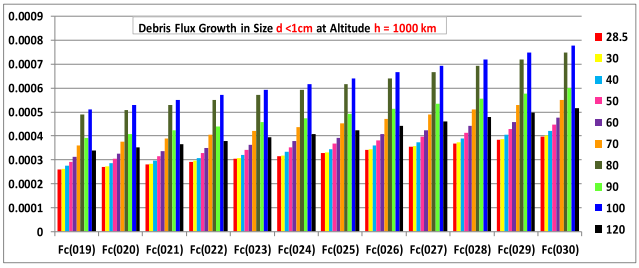

FIGURE 11. Debris flux growth of size $d < 1cm$ at an altitude $h = 1000\ km$ at inclination angles from 28.5 to 120.

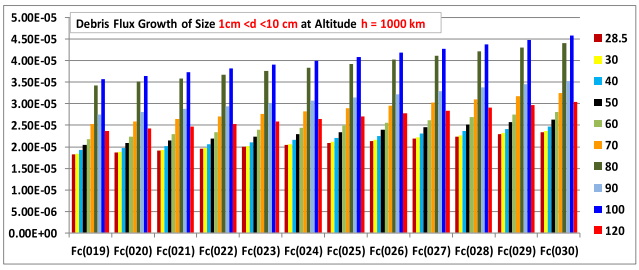

FIGURE 12. debris flux growth of size $1\ cm < d < 10cm$ at altitude $h = 1000\ km$ at inclination angles from 28.5^0 to 120^0.

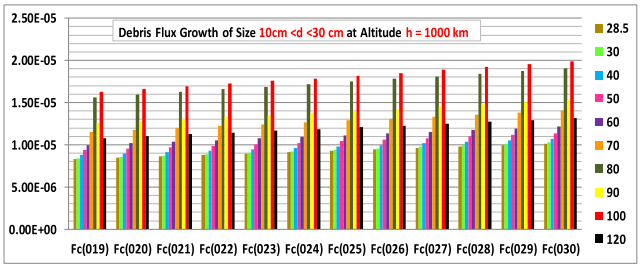

FIGURE 13. debris flux growth of size $10\ cm < d < 30cm$ at altitude $h = 1000\ km$ at inclination angles from 28.5^0 to 120^0.

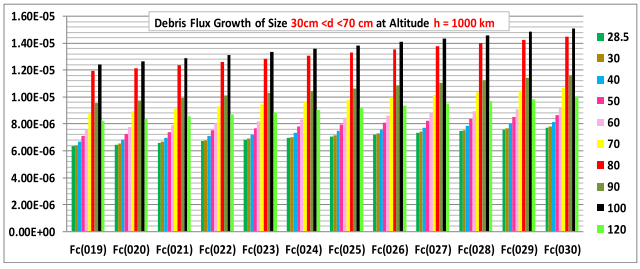

FIGURE 14. debris flux growth of size $30\ cm < d < 70cm$ at altitude $h = 1000\ km$ at inclination angles from 28.5^0 to 120^0.

Regarding the analysis of all debris size patterns at high altitudes, figures 11, 12, 13, 14, 15 and 16 depict the debris flux growth of the six patterns of debris sizes from $d < 1\ cm$ to $d > 120\ cm$ respectively at the altitude $h = 1000\ km$.

The obtained results as shown in these figures explain that there is no large impact of the solar radio flux $F_{10.7}$ within 2023-2026 at high altitudes of satellites' orbits. Moreover, the results show the increasing growth of the debris flux F_C for the six debris size patterns at high altitudes by 2030. In addition, this results confirm also that, all debris sizes

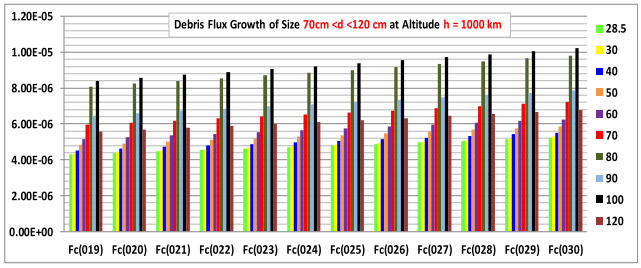

FIGURE 15. debris flux growth of size $70\ cm < d < 120cm$ at altitude $h = 1000\ km$ at inclination angles from 28.5^0 to 120^0.

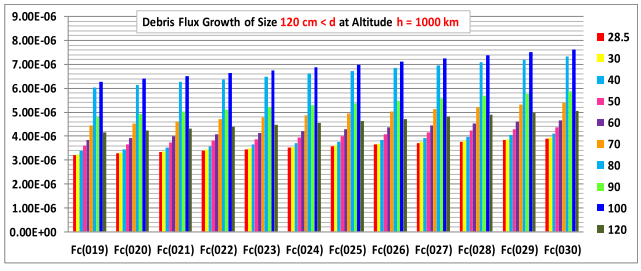

FIGURE 16. debris flux growth of size $120\ cm < d$ at altitude $h = 1000\ km$ at inclination angles from 28.5^0 to 120^0.

patterns are denser at the inclination angles 80^0 and 100^0 than other inclination angles at the high altitudes.

The most striking result to emerge from the previous analysis of the debris flux growth for the six categories of debris sizes is that; all debris sizes are more frequent at the inclination angles 80^0, and 100^0 in the LEO orbits because of the increasing value of the corresponding inclination dependent function $\Psi(i)$. Another interesting finding is the negative correlation between the debris flux growth F_c for all debris sizes and the solar radio flux $F_{10.7}$ within 2023-2026. Moreover, the results clarify and confirm that the debris flux for small size debris $0.5\ cm < d < 70\ cm$ is denser at low and high altitudes, whereas the debris flux for large size debris $d > 70\ cm$ is less dense at low and high altitudes.

B. SATELLITE COLLISION PROBABILITY RESULTS

To validate, support and confirm the obtained results of the debris flux density and growth analysis, the proposed Petri net model for predicting satellite/debris collision probability has been applied on a dataset consisting of eight satellites in LEO orbits at different altitudes. The dataset has been described previously in Table 1.

The results in Tables 2, 3, and 4 show the collision probability calculations for each satellite with the six categories of debris sizes for the years 2019, 2025, and 2030 respectively. The results show that *EnviSat*, and *SuomiNPP* are the most threatened satellites and are predicted to collide with space debris in the next 12 years. As the two satellites orbit at altitudes of 773km, and 834km respectively. This observation confirms that the debris flux is more frequent at the orbits with an inclination angle of $i \simeq 100$, where *EnviSat*, and *SuomiNPP* orbit at the inclination angles of 98.4^0, and 98.7^0 respectively.

TABLE 2. Collision probability *Q(d − size)* results of the eight satellites within 2019.

Satellite	$Q(0.8cm)$	$Q(5cm)$	$Q(20cm)$	$Q(50cm)$	$Q(100cm)$	$Q(140cm)$	$AVG(Q)$
EnviSat	0.022336795	1.58E-03	7.22E-04	5.50E-04	3.73E-04	2.78E-04	4.34E-03
ISS	0.006180574	4.33E-04	1.98E-04	1.51E-04	1.02E-04	7.63E-05	1.19E-03
GRACESat	0.012444165	8.75E-04	4.00E-04	3.05E-04	2.07E-04	1.54E-04	2.41E-03
TiangongSat 2	0.004767669	3.34E-04	1.53E-04	1.16E-04	7.88E-05	5.88E-05	9.20E-04
AQUASat	0.021734496	1.54E-03	7.02E-04	5.35E-04	3.62E-04	2.70E-04	4.22E-03
EO-1 Sat	0.021650655	1.53E-03	6.99E-04	5.33E-04	3.61E-04	2.69E-04	4.20E-03
ICE Sat	0.015239039	1.07E-03	4.91E-04	3.74E-04	2.53E-04	1.89E-04	2.95E-03
Suomi NPP	0.022686942	1.60E-03	7.33E-04	5.58E-04	3.78E-04	2.82E-04	4.41E-03

TABLE 3. Collision probability *Q(d − size)* results of the eight satellites within 2025.

Satellite	$Q(0.8cm)$	$Q(5cm)$	$Q(20cm)$	$Q(50cm)$	$Q(100cm)$	$Q(140cm)$	$AVG(Q)$
EnviSat	0.027126036	1.75E-03	7.80E-04	5.94E-04	4.02E-04	3.00E-04	5.21E-03
ISS	0.003500041	2.24E-04	9.95E-05	7.57E-05	5.13E-05	3.83E-05	6.66E-04
GRACESat	0.009579503	6.14E-04	2.73E-04	2.08E-04	1.41E-04	1.05E-04	1.83E-03
TiangongSat 2	0.002465877	1.58E-04	7.01E-05	5.33E-05	3.61E-05	2.70E-05	4.69E-04
AQUASat	0.02537181	1.64E-03	7.29E-04	5.55E-04	3.76E-04	2.81E-04	4.87E-03
EO-1 Sat	0.025119157	1.62E-03	7.22E-04	5.49E-04	3.72E-04	2.78E-04	4.82E-03
ICE Sat	0.015232788	9.79E-04	4.36E-04	3.31E-04	2.25E-04	1.68E-04	2.91E-03
Suomi NPP	0.028017515	1.81E-03	8.06E-04	6.14E-04	4.16E-04	3.10E-04	5.38E-03

TABLE 4. Collision probability *Q(d − size)* results of the eight satellites within 2030.

Satellite	$Q(0.8cm)$	$Q(5cm)$	$Q(20cm)$	$Q(50cm)$	$Q(100cm)$	$Q(140cm)$	$AVG(Q)$
EnviSat	0.033893973	2.03E-03	8.79E-04	6.68E-04	4.53E-04	3.38E-04	6.45E-03
ISS	0.009170524	5.42E-04	2.35E-04	1.79E-04	1.21E-04	9.02E-05	1.73E-03
GRACESat	0.018677793	1.11E-03	4.81E-04	3.65E-04	2.48E-04	1.85E-04	3.53E-03
TiangongSat 2	0.007052706	4.17E-04	1.80E-04	1.37E-04	9.29E-05	6.93E-05	1.33E-03
AQUASat	0.032954048	1.97E-03	8.54E-04	6.49E-04	4.40E-04	3.28E-04	6.27E-03
EO-1 Sat	0.032822709	1.96E-03	8.51E-04	6.47E-04	4.38E-04	3.27E-04	6.25E-03
ICE Sat	0.023050402	1.37E-03	5.95E-04	4.52E-04	3.06E-04	2.28E-04	4.37E-03
Suomi NPP	0.034435577	2.06E-03	8.93E-04	6.79E-04	4.60E-04	3.43E-04	6.56E-03

The negative correlation between the debris flux and solar radio flux $F_{10.7}$ within 2022-2026 leads to decreased growth if the debris flux at low orbits and altitudes of $h < 600$ *km*. Hence, the results in Table 3 confirms that *ISSsat* and *TiangongSat*2 which orbit at the altitudes 373km and 404 km respectively are the satellites predicted to have the smallest probability of colliding with the space debris. This result also confirms that the debris flux is less frequent in orbits with inclination angles of $i < 60^0$, where, *TiangongSat*2 and *ISSsat* orbit with inclination angles of 42.79^0, and 51.64^0 respectively. Another important result in Tables 2, 3,and 4 is that, the collision probabilities of all satellites have a stronger prediction of colliding with small debris sizes than large debris sizes. However, our results predict the growing rate of the collision probability with large size debris ($d > 30$ *cm*). For example, the collision probability of *Envisat* with debris of size $d > 120cm$ is predicted to grow from 2.78E-04 in 2019 to 3.38E-04 by 2030, and this result contradicts the claim of (Lui,2017)in [18] who said that the collision probability of debris of sizes $d > 10$ *cm* is impossible event.

VI. DISCUSSION

As mentioned in the literature review, prior studies [18] that have noted the importance of analyzing debris flux have observed inconsistent results regarding whether debris can be processed and analyzed as meteoroids. Other studies [6], [12]–[14] have calculated collision probabilities based on position and velocity vectors with respect to the time of the closest approach. However, these studies did not consider predicting the debris flux growth and collision probability for upcoming years. The present study was designed to investigate space debris flux growth in LEO orbits within the period 2019-2030. Moreover, this study set out with the aim of assessing the importance of calculating debris flux at different inclination angles and different altitudes as well as predicting the collision probability with LEO satellites for upcoming years. The current study introduced two Petri net models; The first model can be used for estimating the debris flux in a specific year that has a specific solar radio flux $F_{10.7}$. The model estimates the debris flux with respect to different debris sizes, at different altitudes and with different inclination angles. The second model can be used for calculating the anticipated collision probability of a specific satellite in a given year at an identified altitude and inclination angle. With respect to the first research question about analyzing the debris flux in LEO orbits, small debris sizes of $d < 30$ *cm* are found to be more frequent than large debris sizes. This finding is consistent with that of Lui (2017) who used a meteoroid

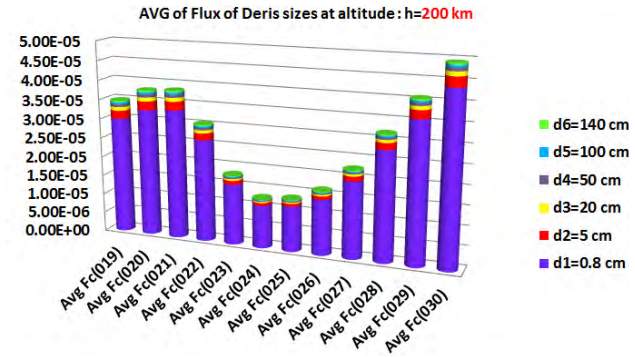

FIGURE 17. Average of debris flux of the six debris sizes at altitude h=200km.

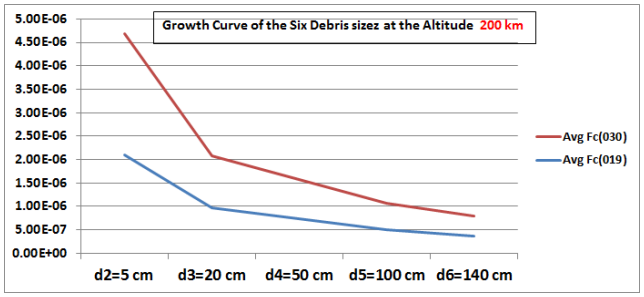

FIGURE 18. Debris flux growth curve at altitude h=200km.

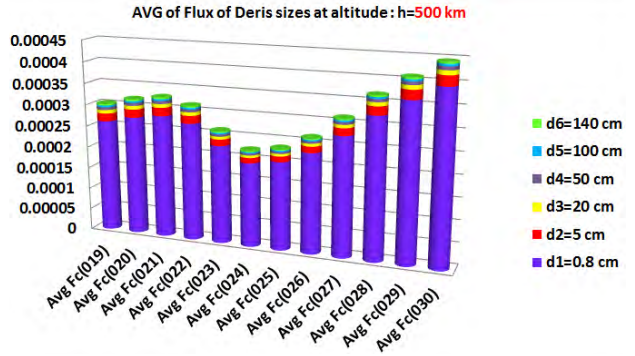

FIGURE 19. Average of debris flux of the six debris sizes at altitude h=500km.

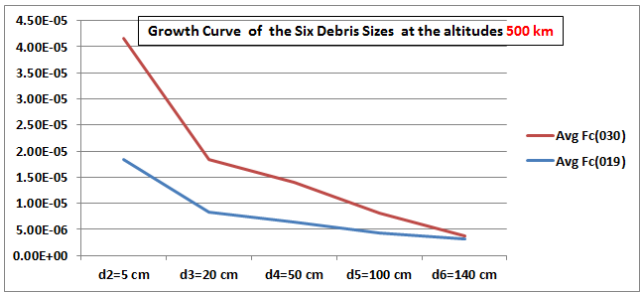

FIGURE 20. Debris flux growth curve at altitude h=500km.

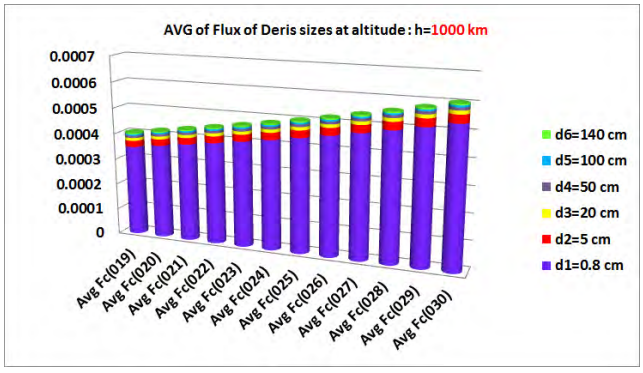

FIGURE 21. Average of debris flux of the six debris sizes at altitude h=1000km.

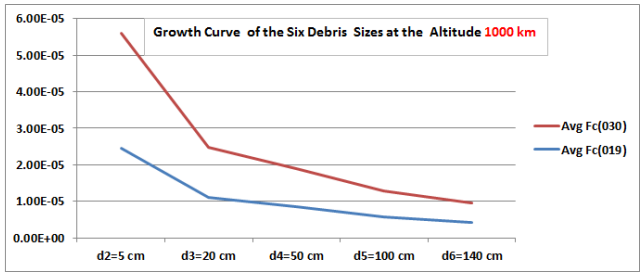

FIGURE 22. Debris flux growth curve at altitude h=1000km.

model for analyzing the debris flux growth [18]. Another important finding was that the decreasing debris flux in low LEO orbits at $h < 600\ km$ within the period 2022 to 2026 is based on a high solar radio flux $F_{10.7}$ value. Figure 17 depicts the debris flux growth rates of all patterns of debris sizes at the altitude of $h = 200\ km$, and Figure 18 compares the growth rates of the debris patterns in the size of $1\ cm < d > 120\ cm$ cm in 2019 with the expected growth rate by 2030 at the altitude of $h = 200\ km$.

Regarding the orbits at the altitude $h = 500\ km$, Figure 19 depicts the debris flux growth rates of the six categories of debris sizes, and Figure 20 compares the growth rate of the six debris sizes $1\ cm < d > 120\ cm$ cm in 2019 with the expected growth rate in 2030. Moreover, Figure 21 depicts the space debris flux growth rates of the six patterns of debris sizes at the altitude of $h = 1000\ km$, and Figure 22 compares the six debris sizes $1\ cm < d > 120\ cm$ cm in 2019 with the expected growth rate in 2030.

With respect to the question of predicting and estimating the collision probabilities of LEO-satellites, this study found that the satellites that orbit at altitudes of $h > 600\ km$ and inclination angles $60^0 < i < 100^0 cm$ are the most threatened by space debris flux, and are predicted to have higher collisions probabilities by 2030 compared to 2019. Figure 23 compares the expected collision probability growth rate of the eight satellites from 2019 to 2030. The depicted result in this figure confirms that *EnviSat*, $EO-1\ Sat$, *SoumiNPPSat*, and *AQUASat* are the satellites predicted to experience the most collisions by 2030. This result also confirms that space debris is more frequent at the altitudes of $600\ km < h < 1000 km$ and inclination angles of $i \simeq 100^0$

Although this study introduced a novel methodology for studying and analyzing space debris flux and predicting

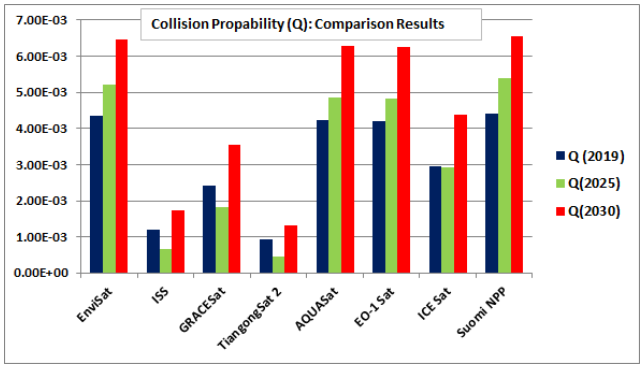

FIGURE 23. Comparison results: The expected collision probability growth of eight LEO satellites between 2019 to 2030.

satellite collisions in LEO orbits, it has been unable to demonstrate its effectiveness in analyzing the flux growth rates in Medium Earth orbit (MEO) or Geosynchronous Equatorial Orbit (GEO). However, these results have not been previously described. Another source of uncertainty is that, although the study introduced an interesting and systematic methodology for analyzing space debris flux, these findings cannot be extrapolated to all debris sizes in space. According to these findings, we can infer that debris flux is rapidly growing and is very dense especially in orbits with inclination angles of $60 < i < 100$. Moreover, the satellite orbits at altitudes of $600\ km < h < 1000km$ and inclination angles of $90 < i < 100$ have higher expected collision values by 2030. This finding has important implications for documenting an important method for modeling and analyzing space debris flux in LEO orbits and predicting satellite collision probability. Despite these promising results, additional research should be undertaken to investigate space debris flux growth in MEO and GEO orbits. Moreover, additional studies, that take this methodology into account, will need to be undertaken to investigate how to prevent the collision between space debris and spacecraft based on smart manoeuvres, which is an important issue.

VII. CONCLUSION

The present study was designed to investigate and analyze space debris flux growth in LEO orbits. The second aim of this study was to investigate the effects of space debris flux when predicting satellite collision probabilities with this debris. This study has introduced two Petri net models for achieving these objectives. The investigation of debris flux growth has shown that debris flux is rapidly growing and very dense especially in orbits with inclination angles of $60 < i < 100$. In addition, this study confirmed that small debris sizes are denser than large ones. Moreover, the satellite orbits at altitudes of $600\ km < h < 1000km$ which have inclination angles of $90 < i < 100$ have greater expected collision values by 2030 than other satellites in low orbits which have inclination angles less than 60^0. Taken together, these findings suggest the role of analyzing debris flux growth in predicting the probability value of satellites collisions with this debris. Overall, the current study provides the first comprehensive assessment and model for space debris flux and prediction of satellite collisions in LEO orbits. Additional Studies need to be carried out to validate the debris flux growth in MEO and GEO orbits. Moreover, further research should focus on determining how to model the behavior of space debris and satellite motions based on invented Petri net models. Moreover, further research should focus on preventing the collisions between space crafts and space debris based on developing smart and effective manoeuvres algorithms.

REFERENCES

[1] J. C. Liou, N. L. Johnson, and N. M. Hill, "Stabilizing the future leo debris environment with active debris removal," *Orbital Debris Quart. News*, vol. 12, no. 4, pp. 5–6, Oct. 2008.
[2] H. G. Lewis, G. G. Swinerd, and R. J. Newland, "The space debris environment: Future evolution," *Aeronaut. J.*, vol. 115, no. 1166, pp. 241–247, 2011.
[3] NASA. (2018). *Space Debris Sensor On Orbit Status Orbital Debris Quarterly News*. [Online]. Available: https://www.orbitaldebris.jsc.nasa.gov/quarterly-news/pdfs/odqnv22i2.pdf
[4] C. T. Shelton and J. L. Junkins, "Probability of collision between space objects including model uncertainty," *Acta Astronaut.*, vol. 155, pp. 462–471, Feb. 2019.
[5] F. K. Chan, *Spacecraft Collision Probability*. Reston, VA, USA: AIAA, 2008, pp. 47–61, 77–98, and 173–190. doi: 10.2514/4.989186.
[6] R. P. Patera, "General method for calculating satellite collision probability," *J. Guid., Control, Dyn.*, vol. 24, no. 4, pp. 716–722, 2001.
[7] M. Yu, S. Li, and S. Leng, "Space collision probability computation based on on-board optical cues," *Acta Astronaut.*, vol. 155, pp. 33–44, Feb. 2019.
[8] S. Le May, S. Gehly, B. A. Carter, and S. Flegel, "Space debris collision probability analysis for proposed global broadband constellations," *Acta Astronaut.*, vol. 151, pp. 445–455, Oct. 2018.
[9] S. Alfano, "A numerical implementation of spherical object collision probability," *J. Astron. Sci.*, vol. 53, no. 1, pp. 103–109, 2005.
[10] R. P. Patera, "Calculating collision probability for arbitrary space vehicle shapes via numerical quadrature," *J. Guid., Control, Dyn.*, vol. 28, no. 6, pp. 1326–1328, Nov. 2005. doi: 10.2514/1.14526.
[11] J. L. Foster, "The analytic basis for debris avoidance operations for the international space station," in *Proc. 3rd Eur. Conf. Space Debris*, Darmstadt, Germany, vol. 473, Mar. 2001, pp. 441–445.
[12] S. Alfano, "Addressing nonlinear relative motion for spacecraft collision probability," in *Proc. AIAA/AAS Astrodyn. Specialist Conf. Exhib.*, Aug. 2006, p. 6760. doi: 10.2514/6.2006-6760.
[13] E. Denenberg and P. Gurfil, "Debris avoidance maneuvers for spacecraft in a cluster," *J. Guid., Control, Dyn.*, vol. 40, no. 6, pp. 1428–1440, 2017.
[14] L. Chen, X. Z. Bai, Y. G. Liang, and K. B. Li, "Calculation of collision probability," in *Orbital Data Applications for Space Objects*. Singapore: Springer, 2017, pp. 135–183.
[15] R. P. Patera, "Satellite collision probability for nonlinear relative motion," *J. Guid., Control, Dyn.*, vol. 26, no. 5, pp. 728–733, 2003.
[16] F. Cérou, P. Del Moral, T. Furon, and A. Guyader, "Rare event simulation for a static distribution," Ph.D. dissertation, INRIA, Paris, France, 2009.
[17] R. Pastel, "Estimating satellite versus debris collision probabilities via the adaptive splitting technique," in *Proc. 3rd Int. Conf. Comput. Modeling Simulation*, Mumbai, India, 2011, pp. 1–6.
[18] M. Liu and Z. Zhu, "Simulation of collision probability between space station and space debris and structure failure probability," *Int. J. Space Sci. Eng.*, vol. 4, no. 3, pp. 253–269, 2017.
[19] NASA. *NASA SSP 30425B Standard*. Accessed: 2018. [Online]. Available: http://everyspec.com/NASA/NASA-JSC/NASA-SSP-PUBS/SSP-30425B-29660/
[20] J.-C. Liou, "Collision activities in the future orbital debris environment," *Adv. Space Res.*, vol. 38, no. 9, pp. 2102–2106, 2006.
[21] J.-C. Liu, D. T. Hall, P. H. Krisko, and J. N. Opiela, "LEGEND—A three-dimensional LEO-to-GEO debris evolutionary model," *Adv. Space Res.*, vol. 34, no. 5, pp. 981–986, 2004.
[22] J. C. Liu, "A statistical analysis of the future debris environment," *Acta Astronaut.*, vol. 62, nos. 2–3, pp. 264–271, 2008.

[23] I. Yuuki, S. Kawamoto, and S. Kibe, "Study on electrodynamic tether system for space debris removal," *Acta Astronaut.*, vol. 55, no. 11, pp. 917–929, 2004.
[24] V. Aslanove and Y. V. and, "Dynamics of large space debris removal using tethered space tug," *Acta Astronaut.*, vol. 91, pp. 149–156, Oct. 2013.
[25] S. I. S. Nishida Kawamoto, Y. Okawa, F. Terui, and S. Kitamura, "Space debris removal system using a small satellite," *Acta Astronaut.*, vol. 56, nos. 1–2, pp. 95–102, 2009.
[26] C. Bombardelli, H. Urrutxua, M. Merino, E. Ahedo, J. Peláez, and J. Olympio, "Dynamics of ion-beam-propelled space debris," in *Proc. 22nd Int. Symp. Space Flight Dyn.*, Sao Jose dos Campos, Brasil, Feb. 2011, pp. 1–13.
[27] C. Bombardelli, H. Urrutxua, M. Merino, J. Pelaez, and E. Ahedo, "The ion beam shepherd: A new concept for asteroid deflection," *Acta Astronaut.*, vol. 90, no. 1, pp. 98–102, 2013.
[28] C. R. Phipps, "A laser-optical system to re-enter or lower low earth orbit space debris," *Acta Astronaut.*, vol. 93, pp. 418–429, Jan. 2014.
[29] C. R. Phipps, K. L. Baker, S. B. Libby, D. A. Liedahl, S. S. Olivier, L. D. Pleasance, A. Rubenchik, J. E. Trebes, E. V. George, B. Marcovici, and J. P. Reilly, "Removing orbital debris with lasers," *Adv. Space Res.*, vol. 49, no. 9, pp. 1283–1300, 2012.
[30] R. Soulard, M. N. Quinn, T. Tajima, and G. Mourou, "ICAN: A novel laser architecture for space debris removal," *Acta Astronaut.*, vol. 105, no. 1, pp. 192–200, 2014.
[31] T. Murata, "Petri nets: Properties, analysis and applications," *Proc. IEEE*, vol. 77, no. 4, pp. 541–580, Apr. 1989.
[32] Natural Environments Branch Solar Activity Forecast. (2018). *Solar Forecast Archive, 13-Month Smoothed Solar Radio 10.7 cm Flux & AP*. [Online]. Available: https://sail.msfc.nasa.gov/index-archive.htm

MOHAMED TORKY is currently a Research Member with the Scientific Research Group in Egypt. He is also with the Department of Computer Science, Higher Institute of Computer Science and Information Systems, Giza, Egypt. His research interests include data mining, and cyber security and modeling

ABOUL ELLA HASSANEIN is currently the Founder and the Head of the Egyptian Scientific Research Group (SRGE) and a Professor of Information Technology with the Faculty of Computer and Information, Cairo University. He is the Ex-Dean of the Faculty of Computers and Information, Beni Suef University. He has more than 1000 scientific research papers published in prestigious international journals and over 45 books covering, such diverse topics as data mining, medical images, intelligent systems, social networks, and smart environment. He is also a member of the Specialized Scientific Council of Information and Communications Technology, Academy of Scientific Research and Technology (ASRT).

AHMED H. EL FIKY is currently pursuing the master's degree with the Faculty of Engineering, Helwan University, Helwan, Egypt. He is also with the Scientific Research Group in Egypt (SRGE).

YAZEED ALSBOU received the B.Sc. degree in electrical engineering from Mutah University, Jordan, in 1997, the M.Sc. degree in telecommunications from the University of Jordan, in 2001, and the Ph.D. degree in computer engineering from Sheffield Hallam University, U.K. He has more than 12 years of teaching experience and research in higher education organizations. He was the Vice Dean of the Deanship of Research, Mutah University, from 2016 to 2018, and the Vice Dean of the Faculty of Engineering, from 2015 to 2016. He is currently a Professor of computer engineering and science with Applied Science University, Bahrain. He is also the acting Dean of Research and Graduate Studies. He joined and represented Mutah University in several projects funded by the European Commission (Erasmus and Erasmus Plus). He has more than 20 research articles and two book chapters published in refereed journals, books, and conferences. His research interests include QoS, computer networks' performance evaluation, image processing, cognitive networking, and cloud computing. He is also serving as a TPC and a Reviewer for several international refereed journals and conferences.